 CMES, vol.93, no.5, pp.335-361, 2013

Accuracy of Quarter-point Element in Modeling Crack-tip Fields

G. P. Nikishkov[1]

Abstract: Accuracy of the quarter-point and transition elements is investigated on one- and two-dimensional problems with inverse square-root singularity. It is demonstrated that most coefficients of the stiffness matrix of the quarter-point element are unbounded. However, numerical integration produces finite values of these coefficients. Influence of several parameters on the error in determining the stress intensity factor is studied. Solution accuracy can be improved using special distribution of element sizes and increasing the element integration order in the radial direction.

Keywords: Finite element method, linear fracture mechanics, quarter-point element.

1 Introduction

The quarter-point singular element has been employed in finite element modeling of crack-tip fields for several decades. It was proposed by Henshell and Shaw (1975) and Barsoum (1976, 1977). They showed that by shifting midside nodes of a quadratic isoparametric element to quarter-side positions it is possible to model exactly square-root singularity of the strains and stresses near the crack tip. Hibbitt (1977) and Ying (1982) demonstrated that the strain energy of a quarter-point element degenerated into a triangle is always bounded. Lynn and Ingraffea (1978) generalized the quarter-point element to the so-called transition element. Transition elements are located in the finite element mesh at some distance from the crack tip and exactly represent the square-root singularity with the pole at the crack tip. Midside nodes of transition elements are placed at positions between quarter- and mid-point. The placement of midside nodes depends on the distance of the transition element from the crack tip.

While this study considers the use of quarter-point elements with the finite ele-

[1] University of Aizu, Aizu-Wakamatsu, Japan.

ment discretization, same elements are employed in other methods that are used in fracture mechanics modeling. For example, Wang and Yao (2011) use shifting of nodes to quarter-point positions in a multipole dual boundary element method for three-dimensional crack problems. Direct computation of stress intensity factors using the displacement discontinuity at the crack face with the quarter-point boundary elements is performed by Nikishkov, Park, and Atluri (2001), Dong and Atluri (2013a) and Dong and Atluri (2013b) who model three-dimensional cracks with the symmetric Galerkin boundary element method.

Some papers have discussed computational aspects of application of quarter-point elements to fracture mechanics problems. Harrop (1982) considered the optimum size of quarter-point crack tip element and stated that the singular element should not be too large since it represents just the inverse square-root and constant terms of the radial stress field. Fawkes, Owen, and Luxmoore (1979) compared several types of singular elements for modeling crack tip fields. They concluded that elements with analytical representation of asymptotic fields and quarter-point elements are both suitable for such purposes. Murti and Valliappan (1986) found that with the use of transition elements, the optimum quarter-point element size is 0.15–0.25 of the crack length for a 5% error bound. Lim, Johnston, and Choi (1991) demonstrated that no optimal transition element size exists. Yavari, Moyer, and Sarkani (1999) showed that for large crack-tip elements using transition elements has no improving effect; however when crack-tip elements are small, transition elements can improve the accuracy. Saouma and Schwemmer (1984) investigated accuracy of the quarter-point element depending on several parameters, including integration order, number of elements around the crack tip, effect of transition elements, and relative size of the singular element. They recommend using two by two integration rules and employing four to eight elements around the crack tip. It was found that transition elements have little effect unless extremely small quarter-point elements are used.

This paper studies accuracy of modeling crack-tip displacement fields using the quarter-point singular element and transition elements. Unlike authors of previous publications where finite cracked specimens were considered, we perform finite element analysis of singularity problems with known solutions.

Our contribution includes the following. One-dimensional problem is proposed which allows to investigate pure radial behavior of the quarter-point element. We demonstrate that most stiffness coefficients of the quarter-point element are unbounded and the integration order does not affect its performance. New distribution of element sizes is proposed. It provides equal radial increments of stresses per element and increases accuracy of the stress intensity factor, especially in cases of small crack-tip elements. It is shown that using more integration points in radial di-

rection of finite elements (except quarter-point elements) provides better accuracy for problems with small crack-tip elements.

The paper is organized as follows. First, the one-dimensional case is investigated using a specially constructed inverse square-root singularity problem. We derive the relation for location of midside node for modeling the singularity in crack-tip and transition elements in a way slightly different from Lynn and Ingraffea (1978). It is demonstrated that coefficients of the stiffness matrix of the quarter-point element are unbounded. However, numerical solution can be obtained due to numerical integration which produces finite stiffness coefficients. New element size distributions are proposed that are based on equal function increment per element and equal derivative of function increment per element. It is shown that solution accuracy can be improved using special distribution of element sizes and increasing integration order for ordinary or transition elements.

An elasticity problem for a circular area near a crack tip with boundary tractions computed from asymptotic stress fields is used for accuracy investigation of a quarter-point element in two-dimensional case. As in the one-dimensional case, stiffness coefficients of the two-dimensional quarter-point element are unbounded except for coefficients in columns an rows related to quarter-point nodes. Computation of the strain energy for a circular crack-tip area using quarter-point elements produces energy values which are very close to the theoretical ones. Special distribution of element sizes in the radial direction and elevated integration order in the radial direction help to improve accuracy of the stress intensity factor computation.

2 One-dimensional singular element

Study of quarter-point and transition elements on one-dimensional problems allows performing some important derivations analytically. When numerical experiments are performed it is easier to investigate influence of problem parameters on results in one-dimensional problems than in problems with two or three dimensions.

2.1 Location of the midside node

Let us consider a one-dimensional boundary value problem with a singular point S on the left of the problem domain. Unknown displacement u has an inverse square root singularity for its derivative $du/dx \sim 1/\sqrt{r}$, where r is distance from the singular point. To use the finite element method to solve this problem it is necessary to model $u \sim \sqrt{r}$ displacement behavior. Modeling $\sqrt{r}$ displacement can be achieved using three-node finite elements with midside nodes shifted from their central positions. Fig. 1 shows a one-dimensional element with three nodes, located at distance s from a singular point and with unit length. Coordinate x and

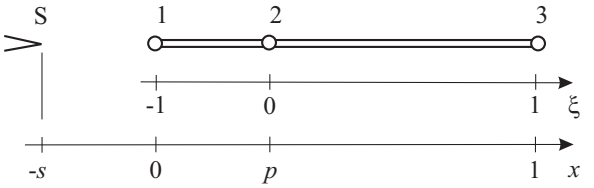

Figure 1: Singularity modeling using shift of a midside node. Displacement derivative du/dx tends to infinity at point S.

displacement u are specified in a parametric form

$$\begin{aligned} x &= \sum N_i x_i \,, \\ u &= \sum N_i u_i \,. \end{aligned} \tag{1}$$

Here x_i, u_i are nodal values of coordinate and displacement. Shape functions N_i are quadratic polynomials of a local coordinate ξ with range $[-1,1]$:

$$\begin{aligned} N_1 &= -\frac{1}{2}\xi(1-\xi), \\ N_2 &= 1-\xi^2, \\ N_3 &= \frac{1}{2}\xi(1+\xi). \end{aligned} \tag{2}$$

If the midside node is located at the element center $p = 0.5$, then coordinate x and displacement u are interpolated by quadratic polynomials of x. Shifting the midside node allows changing interpolation functions expressed through x. To find location p of the midside node that provides modeling of the inverse square root singularity at point $x = -s$, we can take into account that the derivative of displacement with respect to x is infinite at this point:

$$\frac{du}{dx} = \frac{du}{d\xi}\frac{d\xi}{dx} \to \infty \quad \text{at } x = -s. \tag{3}$$

Since derivative $du/d\xi$ is finite for bounded displacements u_i, the displacement derivative approaches zero at the singularity point when

$$\frac{dx}{d\xi}\Big|_{x=-s} = 0. \tag{4}$$

Substituting node coordinates in Equation (1) we obtain the dependence of x on local coordinate ξ,

$$x = (\frac{1}{2} - p)\xi^2 + \frac{1}{2}\xi + p. \tag{5}$$

After differentiation of the above equation, the condition of zero derivative (4) becomes

$$(1-2p)\xi+\frac{1}{2}=0. \tag{6}$$

If the singularity point is at node 1 then location of midside node p can be obtained by substituting $\xi=-1$ into Equation (6):

$$p=\frac{1}{4}. \tag{7}$$

For nonzero value of s it is necessary to express ξ from Equation (6) and substitute it into (5) with $x=-s$. This produces the quadratic equation for parameter p,

$$2p^2-(1-2s)p+\frac{1}{8}-s=0, \tag{8}$$

the appropriate root of which gives the location of the midside node p for the derivative singularity at point S,

$$p=\frac{1}{4}\left(1-2s+2\sqrt{s^2+s}\right). \tag{9}$$

Elements with shifted midside nodes at $p>1/4$ are usually called transition elements. Such elements are located between the singular quarter-point element and ordinary elements in the mesh.

To confirm that the singularity order is correct it is possible to express local coordinate ξ though x and p using (5) and substitute it into second relation of (1). For example, for the quarter-point element $p=1/4$, displacement u depends on x as

$$u=\frac{1}{2}\left(2-3\sqrt{x}+x\right)u_1+\left(2\sqrt{x}-x\right)u_2+\frac{1}{2}\left(x-\sqrt{x}\right)u_3. \tag{10}$$

2.2 Stiffness matrix of the quarter-point element

The stiffness matrix of a one-dimensional finite element is determined by computing the integral over element line L,

$$[k]=\int_L E\left[\frac{dN}{dx}\right]^T\left[\frac{dN}{dx}\right]dx, \tag{11}$$

where E is Young's modulus and $[dN/dx]$ is a vector composed of derivatives of nodal shape functions. Considering that derivatives of shape functions in local and global coordinate systems are related by

$$\left[\frac{dN}{d\xi}\right]=\left[\frac{dN}{dx}\right]\frac{dx}{d\xi}, \tag{12}$$

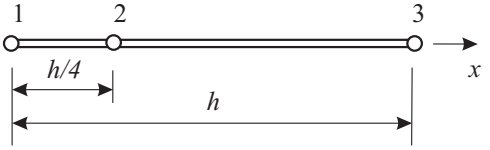

Figure 2: One-dimensional quarter-point element.

the integral for the stiffness matrix in the local coordinate system is

$$[k] = \int_{-1}^{1} E \left[\frac{dN}{d\xi}\right]^T \left[\frac{dN}{d\xi}\right] \left(\frac{dx}{d\xi}\right)^{-1} d\xi, \tag{13}$$

For a quarter-point element of length h, as shown in Fig. 2, derivative $dx/d\xi$ is determined from Equation (5) with $p = 1/4$,

$$\frac{dx}{d\xi} = \frac{h}{2}(1+\xi) \tag{14}$$

and coefficients for integration of the stiffness matrix are

$$[k] = \int_{-1}^{1} \begin{bmatrix} \left(-\frac{1}{2}+\xi\right)^2 & \xi - 2\xi^2 & -\frac{1}{4}+\xi^2 \\ & 4\xi^2 & -\xi - 2\xi^2 \\ \text{Sym} & & \left(\frac{1}{2}+\xi\right)^2 \end{bmatrix} \frac{2E}{h(1+\xi)} d\xi \tag{15}$$

Integration produces the analytical expression for the stiffness matrix of one-dimensional quarter-point element

$$[k] = \frac{E}{2h} \begin{bmatrix} 9G-16 & -12(G-2) & 3G-8 \\ -12(G-2) & 16(G-2) & -4(G-2) \\ 3G-8 & -4(G-2) & G \end{bmatrix}, \tag{16}$$

$G = \log 2 - \log 0.$

All entries of this stiffness matrix are unbounded. However, the quarter-point element correctly models rigid body displacement since the sum of coefficients in any row of the stiffness matrix is zero.

Gauss integration rule is usually used for integration of finite element stiffness matrices, typically with two or three points for quadratic elements. Such integration produces finite values for unbounded stiffness coefficients. Dependence of stiffness coefficient k_{33} on the number of integration points N_G for one-dimensional quarter-point element with $h = 1$ and $E = 1$ is presented in Fig. 3. It can be seen that even for a large number of integration points the stiffness coefficients k_{ij} have modest magnitudes.

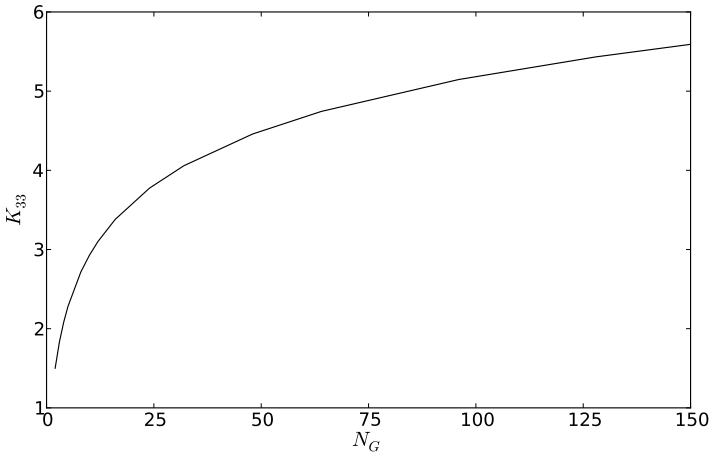

Figure 3: Dependence of the stiffness coefficient k_{33} on the number of Gauss integration points N_G for one-dimensional quarter-point element.

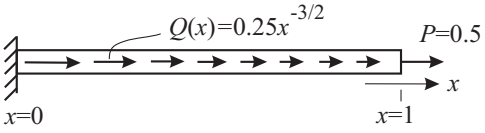

Figure 4: One-dimensional inverse square-root singular problem.

2.3 Solution of one-dimensional singular problem

It is easier to experiment with a quarter-point element in the one-dimensional case. This had never been done before since a crack can not be explicitly introduced in one dimension. We propose an artificially constructed problem where the inverse square-root singularity in function derivative is caused by a distributed load with singularity. This singular problem is shown in Fig. 4. One-dimensional beam has unit length and unit cross-sectional area. It is constrained at $x = 0$ and subjected to singular distributed load $Q(x) = 0.25x^{-3/2}$ and concentrated force $P = 0.5$ at $x = 1$. It is not difficult to check that for Young's modulus $E = 1$ the exact solution of this problem is $u = \sqrt{x}$.

First, the singular problem of Fig. 4 is solved in closed form using one quarter-point finite element with analytical expressions for the stiffness matrix and load vector. The analytical stiffness matrix is given by relation (16). Element load vector $\{f\}$ is

equal to the sum of nodal equivalent of the distributed load plus concentrated force,

$$\{f\} = \int_{-1}^{1} [N]^T Q(\xi) \frac{dx}{d\xi} d\xi + \{p\}, \tag{17}$$

where $[N]$ is a row matrix of the nodal shape functions, $Q(\xi)$ is the distributed load expressed through local coordinate ξ (noting that $x = (1+\xi)^2/4$), and $\{p\}$ is a vector containing concentrated force $P = 0.5$.

Because of displacement constraint for the first node $u_1 = 0$, it is necessary to express equilibrium equations just for nodes 2 and 3. Taking entries of the stiffness matrix (16) and integrating loads (17) for nodes 2 and 3, we arrive at the following equation system:

$$\begin{aligned} 8(G-2)u_2 - 2(G-2)u_3 &= 2(G-1) \\ -2(G-2)u_2 + \frac{1}{2}Gu_3 &= \frac{1}{2}(3-G) \end{aligned} \tag{18}$$

This equation system has the solution:

$$u_2 = \frac{1}{2} + \frac{1}{4(G-2)}, \quad u_3 = 1 \tag{19}$$

The solution approaches the exact results as $G \to \infty$.

It is possible to consider problem solution using one singular quarter-point element and several ordinary elements. An equation system is assembled from element contributions. Analysis of the elimination process for unknowns indicates that G entries eliminate each other inside the quarter-point element and do not propagate to other elements. Thus the solution is independent of G except for the displacement value at the quarter-point node u_2. Since the solution does not depend on the G value then the number of integration points for estimation of stiffness matrix of quarter-point element does not affect results of the singular problem provided that we do not use one-point integration.

2.4 Distribution of nodes near singular point

When the singular quarter-point element is used together with ordinary quadratic elements or transition elements, the solution can be affected by both singular element size and size distribution of other elements. In some publications such as [Barsoum (1977)], element size distribution follows an arithmetic progression with first term equal to the quarter-point element size. We propose to consider two element size distributions based on constant displacement difference and constant displacement derivative difference per element. Later it will be demonstrated that constant displacement difference per element produces elements with sizes described by arithmetic progression.

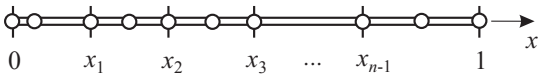

Figure 5: Distribution of n elements over the interval $[0,1]$. The size of the first (singular) element is x_1.

Constant derivative difference per element can be related to an error indicator [Zienkiewicz (2005)] that is based on an averaging of the nodal solution for neighboring finite elements. The stress at the node can be obtained as a weighted least squares approximation using the reduced integration points in elements around the node. The difference between the finite element solution and the least squares approximation at the node gives an estimate of the local error. For larger solution gradient change, the local error becomes larger. Equal derivative difference per element can provide approximately equal local errors.

Let us find placement of element boundaries for n three-node elements on interval $[0,1]$, as shown in Fig. 5. The size of the singular quarter-point element is x_1. It is required to find placement of element boundaries $x_1 \ldots x_{n-1}$ based on adopted conditions.

2.4.1 Constant displacement increment per element

The condition of constant displacement increment per element leads to the following equation for element boundaries:

$$\sqrt{x_{i+1}} - \sqrt{x_i} = \frac{1}{n}. \tag{20}$$

The evident solution of this equation is a quadratic function for location of element boundaries

$$x_i = \left(\frac{i}{n}\right)^2. \tag{21}$$

According to quadratic solution, the singular element size is $1/n^2$ and element sizes follow an arithmetic progression. Thus using arithmetic progression for element sizes in the vicinity of the square-root singular point means constant increment of displacement per element, which has no justification from accuracy point of view.

If sizes of several first elements are already defined, then next element boundary location is determined by the equation

$$\sqrt{x_{i+1}} - \sqrt{x_i} = \frac{1 - \sqrt{x_i}}{n - i}. \tag{22}$$

Solving this equation with respect to x_{i+1}, we obtain a recurrent relation for element boundaries

$$x_{i+1} = \left(\frac{1 + (n-i-1)\sqrt{x_i}}{n-i} \right)^2 . \tag{23}$$

When size of the quarter point element is specified not equal to $1/n^2$, the above relation allows determination of sizes of all other elements to satisfy the condition of constant function increment.

2.4.2 Constant displacement derivative increment per element

The second criterion for subdivision of the interval $[0,1]$ into finite elements is based on constant difference of displacement derivative per element. Since derivative $du/dx = 1/(2\sqrt{x})$ is infinite at point $x = 0$ the size of the singular element x_1 should be specified. Locations of element boundaries $x_2 \ldots x_{n-1}$ can be found from the condition

$$\frac{1}{\sqrt{x_{i+1}}} - \frac{1}{\sqrt{x_i}} = \frac{1}{n-i} \left(1 - \frac{1}{\sqrt{x_i}} \right), \tag{24}$$

which provides the following expression for x_{i+1}:

$$x_{i+1} = \left(\frac{(n-i)\sqrt{x_i}}{(n-i-1) + \sqrt{x_i}} \right)^2 \tag{25}$$

If the singular element size is $x_1 = 1/n^2$, then locations of element boundaries x_i are described by the rational function

$$x_i = \left(\frac{1}{n+1-i} \right)^2 . \tag{26}$$

Comparison of placement of element boundaries x_i according to criteria of constant displacement derivative increment and constant displacement increment is shown in Fig. 6 for different sizes of singular elements 0.01, 0.1, and 0.2.

2.5 Investigation of accuracy

The problem presented in Section 2.3 and illustrated in Fig. 4 is used to investigate solution accuracy using one singular quarter-point element and several ordinary or transition elements. Since quarter-point and transition elements can model a solution precisely, then using appropriate finite element parameters, we should be able to obtain results with errors due to restricted mantissa in the computer representation of numbers. The one-dimensional solution domain [0, 1] is discretized into

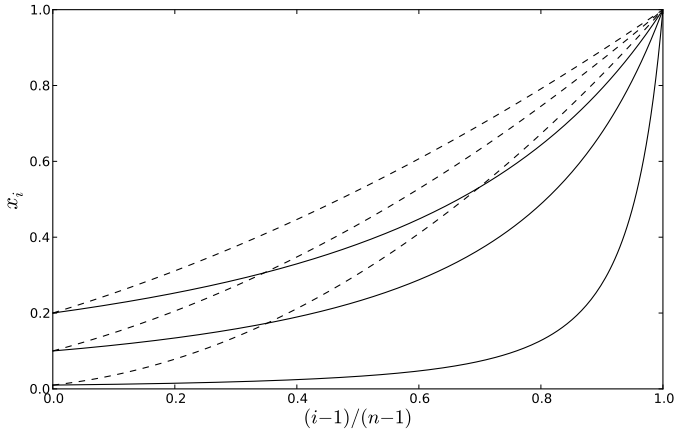

Figure 6: Coordinate of element boundaries x_i as a function of element number i for different sizes of singular elements ($x_1 = 0.01$, 0.1, and 0.2). Solid lines: equal increments of displacement derivative, dashed lines: equal increments of displacement.

eight elements ($n = 8$), comprising one quarter point elements and seven ordinary or transition elements.

Influence of the following parameters on the solution precision is investigated:

Quarter-point element size h;

Number of Gauss integration points in elements (excepting the quarter-point element);

Element types – ordinary or transition elements in addition to the quarter-point element;

Distribution of element sizes – arithmetic progression (AP), equal function increment per element (EF), or equal derivative increment per element (ED);

Results of finite element solution of the one-dimensional inverse square-root singular problem are presented in Table 1 as error of displacement at node located at $x_1 = h$. While indirect estimation of displacement at the quarter-point node is possible on the basis of (19), we prefer to use direct value at the right end of the quarter-point element. Computation of the stiffness matrix of the quarter-point element is always performed using two Gauss integration points, since the solution does not depend on the integration precision (except the quarter-point node that we

Table 1: Errors (percent) in solution of one-dimensional singular problem. Solution domain [0, 1] is divided into one quarter-point element of size h and seven ordinary or transition elements. Elements (except quarter-point) are integrated with N_G Gauss integration points. Element subdivisions: AP – arithmetic progression, EF – equal function difference per element, ED – equal derivative difference per element.

		Q-point and ordinary elements			Q-point and transition elements		
h	N_G	AP	EF	ED	AP	EF	ED
1/8	2	-0.0461	-0.0093	-0.0055	0.0096	-0.0071	-0.0041
1/8	3	-0.0016	-1.32e-04	-6.85e-05	-9.88e-04	-1.68e-04	-2.97e-06
1/8	8	-5.85e-11	-1.26e-13	-2.81e-12	9.03e-12	-4.87e-13	-2.34e-12
1/64	2	-1.0266		-0.2921	0.4595		-0.0500
1/64	3	-0.1373		-0.0356	-0.0495		-1.92e-04
1/64	8	-3.82e-06		-9.55e-07	-2.70e-08		-9.96e-11
1/64	16	-3.89e-13		-3.54e-11	-6.00e-13		-3.36e-11
1/512	2	-14.0280	-12.0054	-2.3113	5.2445	5.2267	-0.5891
1/512	3	-7.1735	-5.6140	-1.0258	1.6200	1.0949	-0.0849
1/512	8	-0.1380	-0.0685	-0.0123	0.0014	6.12e-04	-7.55e-07
1/512	16	-1.39e-04	-3.39e-05	-6.13e-06	-8.66e-09	-1.07e-09	-1.18e-09
1/512	32	-9.54e-11	-5.89e-12	-1.18e-09	-1.73e-13	-1.57e-14	-1.18e-09

ignore). Results for the EF element distribution with $h = 1/64$ are not given in the table since for $h = 1/n^2$ the element distributions AP and EF are exactly same and results are also same.

After analysis of Table 1 we conclude that:

Solution error increases with decrease of the quarter-point element size provided that constant number of elements is used;

Solution accuracy becomes higher with increase of number of Gauss integration points N_G for evaluation of element stiffness matrices;

Use of transition elements increases solution accuracy compared to that using ordinary elements;

Distribution of element boundaries according to the criterion of equal derivative difference per element (ED) provides better accuracy compared to other element boundary placements.

From an accuracy point of view, the most favorable quarter-point element size is $h = 1/n$, where n is the number of elements. However, even in this case the use of transition elements and ED element subdivision reduce solution error by ten times for number of integration points $N_G = 2$ compared to using elements of equal size. Using Gauss integration $N_G = 8$ provides a practically precise solution (since computer mantissa contains 15 digits, the error $10^{-13}\%$ corresponds to machine precision). Using more Gauss integration points for stiffness evaluation (up to $N_G = 32$), it is possible to have almost maximally precise results in all cases. Using small number of integration points, as usually done in finite element modeling, can lead to considerable errors for smaller sizes of the quarter-point element. For $h = 1/n^2$ and $N_G = 2$ the error is larger than 1% for ordinary elements with arithmetic progression distribution (AP). Decrease of the singular element size to $h = 1/n^3$ causes 14% solution error for the same number of integration points and element distribution.

The universal recipe for obtaining accurate solution results of the one-dimensional singular problem includes using transition elements with ED distribution of element sizes and eight Gauss points for integration of element stiffness matrices.

3 Two-dimensional singular element

In linear elastic fracture mechanics, the state of a symmetrical crack is characterized by a stress intensity factor that is a scaling coefficient for the crack-tip asymptotic fields. Accuracy of the stress intensity factor depends upon the quality of representation of the asymptotic displacement and stress fields. Two-dimensional singular quarter-point elements are routinely used for modeling crack-tip fields. Results of modeling depend on finite element types and finite element mesh. We explore here stiffness matrix of the quarter-point element, computation of strain energy in the near crack tip region, and accuracy of stress intensity factor determination.

3.1 Stiffness matrix of the quarter-point element

Consider a two-dimensional quarter-point element shown in Fig. 7. The element has size h in x-direction and size $2l$ in y-direction. Nodes 1, 7, and 8 are located at the xy coordinate origin, and midside nodes 2 and 6 are shifted to quarter-side positions. The element has symmetry with respect to x-axis.

Stiffness matrix of the element of Fig. 7 can be obtained in closed form. We are not going to derive analytical expressions for entries of the stiffness matrix because they are cumbersome. Instead we want to investigate whether stiffness matrix entries are bounded or not. Coefficients of the stiffness matrix $[k]$ for two-dimensional isoparametric elements can be expressed as:

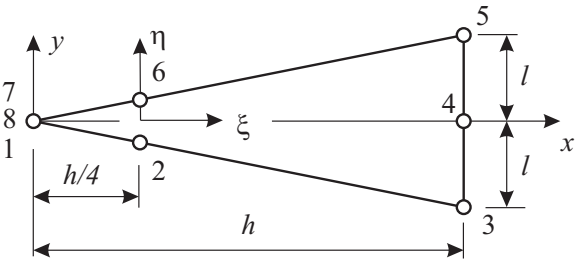

Figure 7: Two-dimensional quarter-point element.

$$k_{ii}^{mn} = \int_{-1}^{1}\int_{-1}^{1} \left((\lambda + 2\mu) \frac{\partial N_m}{\partial x_i} \frac{\partial N_n}{\partial x_i} + \mu \frac{\partial N_m}{\partial x_{i+1}} \frac{\partial N_n}{\partial x_{i+1}} \right) \det J \, d\xi d\eta,$$
$$k_{ij}^{mn} = \int_{-1}^{1}\int_{-1}^{1} \left(\lambda \frac{\partial N_m}{\partial x_i} \frac{\partial N_n}{\partial x_j} + \mu \frac{\partial N_m}{\partial x_j} \frac{\partial N_n}{\partial x_i} \right) \det J \, d\xi d\eta. \tag{27}$$

Here k_{ij}^{mn} are stiffness matrix coefficients with subscripts ij corresponding to coordinates xy and superscripts mn corresponding to local node numbers from 1 to 8, λ and μ are the Lame constants, $\det J$ is the determinant of the Jacobian matrix, and N_i are nodal shape functions depending on local coordinates ξ, η:

$$\begin{aligned}
N_i &= \frac{1}{4}(1+\xi\xi_i)(1+\eta\eta_i) - \frac{1}{4}(1-\xi^2)(1+\eta\eta_i) - \frac{1}{4}(1+\xi\xi_i)(1-\eta^2),\ i = 1,3,5,7 \\
N_i &= \frac{1}{2}(1-\xi^2)(1+\eta\eta_i)\ ,\ \ i = 2,\ 6 \\
N_i &= \frac{1}{2}(1+\xi\xi_i)(1-\eta^2)\ ,\ \ i = 4,\ 8
\end{aligned} \tag{28}$$

where ξ_i, η_i are local coordinate values at node i.

Transformation of derivatives of shape functions from the local coordinate system ξ, η to the global coordinates x, y is performed with the use of the Jacobian matrix $[J]$

$$\begin{Bmatrix} \frac{\partial N_i}{\partial x} \\ \frac{\partial N_i}{\partial y} \end{Bmatrix} = [J]^{-1} \begin{Bmatrix} \frac{\partial N_i}{\partial \xi} \\ \frac{\partial N_i}{\partial \eta} \end{Bmatrix}, \qquad [J] = \begin{bmatrix} \frac{\partial x}{\partial \xi} & \frac{\partial y}{\partial \xi} \\ \frac{\partial x}{\partial \eta} & \frac{\partial y}{\partial \eta} \end{bmatrix}. \tag{29}$$

Using Equation (1) with shape functions (28) it is possible to express coordinate x through ξ; coordinate y is linearly related to x through η [Barsoum (1977)]:

$$\begin{aligned} x &= \frac{1}{4}h(1+\xi)^2, \\ y &= \frac{1}{4}l(1+\xi)^2\eta. \end{aligned} \tag{30}$$

Differentiation of the above relations for x and y with respect to ξ and η produces the Jacobian matrix

$$[J] = \begin{bmatrix} h(1+\xi)/2 & l(1+\xi)\eta/2 \\ 0 & l(1+\xi)^2/4 \end{bmatrix}. \tag{31}$$

The determinant of the Jacobian matrix and its inverse are

$$\det J = \frac{1}{8}hl(1+\xi)^3, \tag{32}$$

$$[J]^{-1} = \frac{2}{hl(1+\xi)^2}\begin{bmatrix} l(1+\xi) & -2l\eta \\ 0 & 2h \end{bmatrix}. \tag{33}$$

To estimate stiffness coefficient k_{11}^{11}, derivatives $\partial N_1/\partial x$ and $\partial N_1/\partial y$ are needed, which can be obtained with differentiation of shape function N_1 and use of the inverse of the Jacobian matrix,

$$\begin{aligned} \frac{\partial N_1}{\partial x} &= \frac{1}{2h(1+\xi)^2}\left[(1+\xi)(1-\eta)(2\xi+\eta)-\eta(1-\xi)(\xi+2\eta)\right], \\ \frac{\partial N_1}{\partial y} &= \frac{1}{l(1+\xi)^2}(1-\xi)(\xi+2\eta). \end{aligned} \tag{34}$$

It is easy to see that the stiffness coefficient k_{11}^{11} can be presented as

$$\begin{aligned} k_{11}^{11} &= \int_{-1}^{1}\int_{-1}^{1}\left((\lambda+2\mu)\left(\frac{\partial N_1}{\partial x}\right)^2+\mu\left(\frac{\partial N_1}{\partial y}\right)^2\right)\det J\, d\xi d\eta \\ &= \int_{-1}^{1}\int_{-1}^{1}\frac{f(\xi,\eta)}{1+\xi}d\xi d\eta, \end{aligned} \tag{35}$$

where $f(\xi,\eta)$ is a polynomial function of ξ,η that does not contain multiplier $(1+\xi)$. Using Mathematica (2010) it is possible to confirm that indefinite integrals of both $(\partial N_1/\partial x)^2\det J$ and $(\partial N_1/\partial y)^2\det J$ include terms with $\log(1+\xi)$. Result

of evaluation of (35) contains the term $G = (\log 2 - \log 0)$, thus making the stiffness coefficient unbounded.

Derivatives $\partial N_2/\partial x$ and $\partial N_2/\partial y$ for computing coefficient k_{11}^{22} are

$$\begin{aligned} \frac{\partial N_2}{\partial x} &= \frac{2}{h(1+\xi)}\left[\xi(1-\eta)+\eta(1-\xi)\right], \\ \frac{\partial N_2}{\partial y} &= -\frac{2}{l(1+\xi)}(1-\xi), \end{aligned} \tag{36}$$

and the stiffness coefficient results in

$$\begin{aligned} k_{11}^{22} &= \int_{-1}^{1}\int_{-1}^{1}\left((\lambda+2\mu)\left(\frac{\partial N_2}{\partial x}\right)^2+\mu\left(\frac{\partial N_2}{\partial y}\right)^2\right)\det J\, d\xi d\eta \\ &= \int_{-1}^{1}\int_{-1}^{1}(1+\xi)f(\xi,\eta)d\xi d\eta. \end{aligned} \tag{37}$$

Thus coefficient k_{11}^{22} is bounded.

In a similar way it is possible to consider all coefficients of the stiffness matrix. After doing so we find that four columns and four rows related to quarter-side nodes 2, 6 k_{ij}^{2n}, k_{ij}^{m2}, k_{ij}^{6n} and k_{ij}^{m6} contain bounded coefficients; all other coefficients are unbounded. It is interesting that finite values of stiffness coefficients related to quarter-point nodes 2 and 6 are due to presence of multiplier $(1+\xi)$ in shape functions N_2 and N_6. This makes displacements of the quarter-point nodes independent of stiffness integration order.

3.2 Elastic energy

Let us consider a circular region of radius R around a tip of a crack which is located along the negative part of x-axis, as shown in Fig. 8a. Elastic strain-energy density w for plane strain conditions is

$$w = \frac{1}{4\mu}\left[(1-\nu)\left(\sigma_r^2+\sigma_\theta^2\right)-2\nu\sigma_r\sigma_\theta+2{\tau^2}_{r\theta}\right], \tag{38}$$

where μ and ν are the shear modulus and Poisson's ratio, and σ_r, σ_θ, and $\tau_{r\theta}$ are stresses in the polar coordinate system which are controlled by the stress intensity factor K_{I}:

$$\sigma_{ij} = \frac{K_{\mathrm{I}}}{\sqrt{2\pi r}}f_{ij}(\theta)\,, \qquad \left\{\begin{array}{c} f_r \\ f_\theta \\ f_{r\theta} \end{array}\right\} = \cos\frac{\theta}{2}\left\{\begin{array}{c} 1+\sin^2\dfrac{\theta}{2} \\ \cos^2\dfrac{\theta}{2} \\ \sin\dfrac{\theta}{2}\cos\dfrac{\theta}{2} \end{array}\right\}. \tag{39}$$

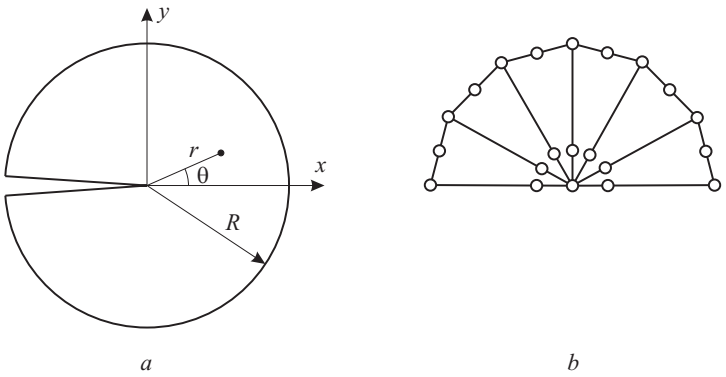

a *b*

Figure 8: Circular region around the crack tip (a) and the finite element model for its symmetric part (b).

Strain energy W for the crack-tip region of radius R is given by the integral

$$W = \int_{-\pi}^{\pi} \int_{0}^{R} w\, r\, dr d\theta = \int_{-\pi}^{\pi} \frac{K_I^2 R}{8\pi\mu} \left[(1-\nu) \left(f_r^2 + f_\theta^2 \right) - 2\nu f_r f_\theta + 2 f_{r\theta}^2 \right] d\theta. \tag{40}$$

Fulfilling the integration we arrive at the following formula for the strain energy under *plane strain* conditions

$$W = \frac{K_I^2 R\,(5-8\nu)}{16\mu}. \tag{41}$$

The elastic strain energy under *plane stress* conditions can be obtained by replacing ν with $\nu/(1-\nu)$:

$$W = \frac{K_I^2 R(5-3\nu)}{16\mu(1+\nu)}. \tag{42}$$

Numerical estimation of elastic energy in a circular region near the crack tip is done using several singular quarter-point elements for a semicircular area, as depicted in Fig. 8b. Values of elastic energy W for a circular region are computed as a sum over all elements,

$$W = \frac{1}{2} \sum_e \{u\}^T [k] \{u\}, \tag{43}$$

Table 2: Elastic energy for a circular region around crack tip ($K_{\mathrm{I}} = 1$, $R = 1$, $\mu = 1$, $\nu = 0.3$, plane strain) computed with different number of elements using different number of integration points N_G.

	4 elements		8 elements		16 elements	
N_G	Straight	Curved	Straight	Curved	Straight	Curved
2	0.155998	0.167555	0.160774	0.163740	0.162062	0.162809
3	0.156104	0.167529	0.160781	0.163738	0.162063	0.162808
32	0.156104	0.167529	0.160781	0.163738	0.162063	0.162808
Eq. (41)	0.154188	0.162500	0.160414	0.162500	0.161978	0.162500

where $[k]$ is element stiffness matrix and $\{u\}$ is element vector of nodal displacements computed from the asymptotic field

$$u_i = \frac{K_{\mathrm{I}}}{\mu}\sqrt{\frac{r}{2\pi}}F_i(\theta)\,, \quad \left\{ \begin{array}{c} F_x \\ F_y \end{array} \right\} = \left\{ \begin{array}{c} \cos\dfrac{\theta}{2} \\ \sin\dfrac{\theta}{2} \end{array} \right\} \left(\frac{\kappa+1}{2} - \cos^2\frac{\theta}{2} \right) \tag{44}$$

$$\kappa = \begin{cases} 3-4\nu & \text{plane strain} \\ (3-\nu)/(1+\nu) & \text{plane stress} \end{cases} \tag{45}$$

Here u_i are displacement components u_x and u_y, r is the distance from the crack tip, and K_{I} is the stress intensity factor.

The following conditions are specified for computation of the elastic energy: stress intensity factor $K_{\mathrm{I}} = 1$, radius of a circular region around the crack tip $R = 1$, shear modulus $\mu = 1$, Poisson's ratio $\nu = 0.3$, plane strain conditions. Elastic energy values are given in Table 2 for 4, 8, and 16 quarter-point elements used in problem discretization. Different number of Gauss points $N_G = 2$, 3, and 32 are employed for integration of element stiffness matrices. Either elements with all straight sides or elements that have one curved side with nodes located on the circle boundary can be present in the mesh. Theoretical values of the elastic energy are calculated according to formula (41). Radii R for theoretical values corresponding to elements with straight sides are computed from the condition of equal areas in the theoretical case and finite element modeling.

Coefficients of element stiffness matrices (except entries in rows and columns related to quarter-point nodes) change considerably with change of Gauss integration rule. However, elastic energy values are practically independent of the number of

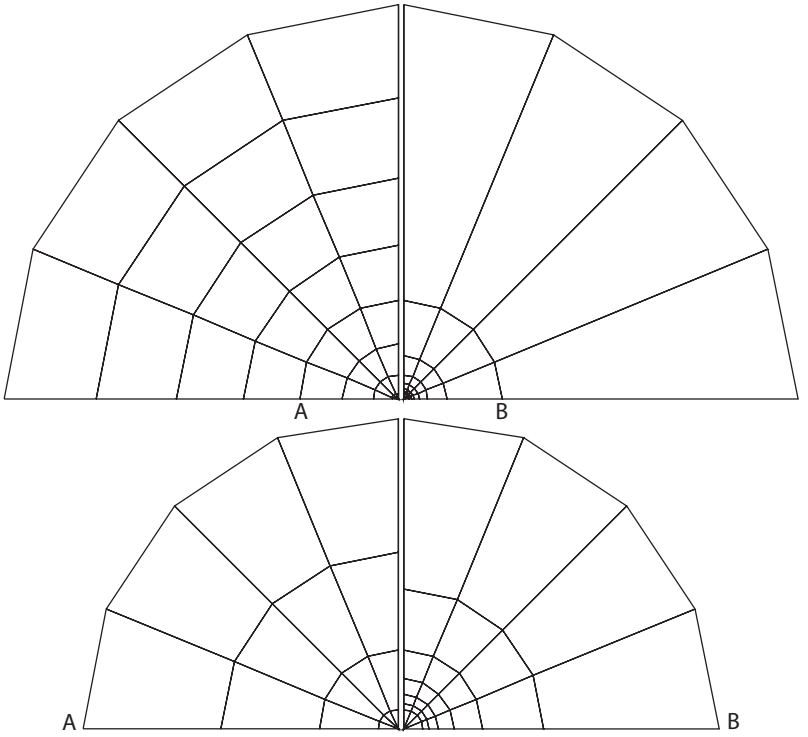

Figure 9: Comparison of meshes with eight elements in the radial direction and quarter-point element size $h = 1/64$: left – arithmetic progression in radial element sizes, right – equal element increment of strains and stresses along radial rays.

integration points. That means that fractions of stiffness coefficients that depend on the integration rule compensate for each other during calculation of the energy quadratic form. The elastic energy results have almost same precision for elements with both straight and curved sides. As can be expected, precision of results increases with increase of number of elements. It is well known that energy methods like the equivalent domain integral method [Nikishkov and Atluri (1987)] provide estimates of the stress intensity factor with high precision.

3.3 Stress intensity factor

Study of accuracy of computation of the stress intensity factor K_{I} is performed on an asymptotic problem for a circular region around the crack tip, as shown in Fig. 8a. Tractions corresponding to the asymptotic stress distribution under *plane*

strain conditions are prescribed at the circle boundary. The symmetric semicircular part of unit radius $R = 1$ is discretized with a polar mesh of n_r by n_θ elements – n_r elements in the radial direction and n_θ elements in the circumferential direction. Singular quarter-point elements surround the crack tip, the remaining elements can be of ordinary or transition types. Distribution of element sizes in the radial direction can be of different types. Fig. 9 illustrates two examples of meshes – arithmetic progression in radial element sizes and equal element increment of strains and stresses along radial rays.

3.3.1 Methods for K_{I} determination

Two methods are used for determination of the stress intensity factor K_{I}: asymptotic displacement method and energetic equivalent domain integral method.

The *displacement method* is based on the asymptotic distribution of displacements near the crack tip (44). Values of the stress intensity factor K_{I} are determined with the use of finite element displacement u_y at a quarter-point node located at $r = h/4$, $\theta = \pi$ (h is the radial size of the quarter-point element):

$$K_{\mathrm{I}} = u_y \frac{E}{1-\nu^2}\sqrt{\frac{\pi}{2h}}, \tag{46}$$

where E and ν are Young's modulus and Poisson's ration, plane strain conditions are assumed.

The *equivalent domain integral method* (EDI) [Nikishkov and Atluri (1987)] is used for computing the J-integral magnitude

$$J = \int\limits_{\Gamma_\varepsilon} \left(w n_x - \sigma_{ij} \frac{\partial u_i}{\partial x} n_j \right) d\Gamma. \tag{47}$$

Here w is the strain energy density, σ_{ij} are stresses, u_i are displacements, n_j are components of the external normal to contour Γ_ε that surrounds the crack tip.

Contour integration can be replaced by area (domain) integration which is more suitable for the finite element method and provides better accuracy:

$$J = \int\limits_{A-A_\varepsilon} \left(w \frac{\partial s}{\partial x} - \sigma_{ij} \frac{\partial u_i}{\partial x} \frac{\partial s}{\partial x_j} \right) dA. \tag{48}$$

Integration area $A - A_\varepsilon$ is between contour Γ_ε and another contour Γ which is farther from the crack tip. A smooth function s has unit value at contour Γ_ε and zero value at outer contour Γ. Under plane strain conditions the stress intensity factor

K_{I} is determined as

$$K_{\mathrm{I}} = \sqrt{\frac{JE}{1-\nu^2}}. \tag{49}$$

In our study, the s function is linear in radial direction and area $A - A_\varepsilon$ corresponds to the second element ring that is next to the ring of quarter-point elements. Plane strain conditions are applied.

3.3.2 Convergence of K_{I} with mesh refinement

We start with convergence study using meshes of n by n elements. Relative radius of the quarter-point elements is $h = 1/n$. Three types of radial distribution of element sizes are employed during mesh generation – arithmetic progression (AP), equal displacement difference per element (EF) and equal stress and strain difference per element (ED). In addition to quarter-point elements, finite element meshes contain ordinary or transition elements. Element stiffness matrices are integrated with two Gauss points in both directions of the local coordinate system ξ, η.

Errors in the stress intensity factor K_{I} for different meshes are presented in Table 3. For small meshes, results do not differ for different distributions of element sizes and different element types. This outcome is expectable (based on experience with one-dimensional analysis) since the quarter-point element size is large enough. For larger meshes it is possible to see differences in convergence. The EDI method provides much better results than the displacement methods. The K_{I} error can be ten and more times less when the EDI method is used. Table 3 includes results for elements with curved sides in the circumferential direction where midside nodes are located at circular arcs. Errors in K_{I} for such meshes is considerably higher than for elements with straight sides. It is recommended to use meshes composed of elements with all straight sides.

3.3.3 Radial distribution of element sizes and integration order

Reasonable K_{I} error less than 0.3% by the displacement method is obtained for meshes of 8×8 elements. This number of elements is selected for further investigation of solution accuracy depending on several parameters.

Similar to the one-dimensional analysis, we study accuracy of the stress intensity factor K_{I} for two-dimensional meshes with the following varying parameters:

Quarter-point element size h;

Method of K_{I} estimation – asymptotic displacement method or energetic EDI method;

Table 3: Errors (percent) in K_{I} values for the two-dimensional asymptotic problem. The mesh consists of $n \times n$ elements. The radius of the quarter-point elements is $1/n$. The rest of the semi-circular area is discretized by ordinary elements. Radial element subdivisions: AP – arithmetic progression, EF – equal function difference per element, ED – equal derivative difference per element.

		Displacement method			EDI method		
$n \times n$	Curved	AP	EF	ED	AP	EF	ED
3×3		-2.917	-2.952	-2.972	-0.029	-0.048	-0.073
4×4		-1.429	-1.444	-1.440	-0.110	-0.106	-0.104
4×4	c	-3.345	-3.325	-3.241	-0.697	-0.674	-0.638
6×6		-0.531	-0.543	-0.525	-0.071	-0.052	-0.037
6×6	c	-1.480	-1.467	-1.402	-0.240	-0.217	-0.195
8×8		-0.263	-0.279	-0.264	-0.048	-0.025	-0.012
8×8	c	-0.813	-0.810	-0.765	-0.120	-0.096	-0.082
16×16		-0.035	-0.060	-0.055	-0.030	-0.004	0.001
24×24		0.003	-0.025	-0.023	-0.028	-0.001	0.001
32×32		0.016	-0.014	-0.013	-0.027	-0.001	0.001
48×48		0.025	-0.006	-0.005	-0.027	-0.0002	0.0005
64×64		0.028	-0.003	-0.003	-0.027	-0.0001	0.0003

Number of Gauss integration points in the radial direction for element stiffness evaluation (except for quarter-point elements);

Element types – ordinary or transition elements in addition to the quarter-point elements;

Distribution of element sizes – arithmetic progression (AP), equal function increment per element (EF), and equal derivative increment per element (ED);

Behavior of the quarter-point element does not depend on the integration order of its stiffness matrix. Because of this quarter-point elements are always integrated with a two by two Gauss rule. Stiffness matrices of other elements (ordinary or transition) are evaluated using two Gauss integration points in the circumferential direction and variable number of integration points N_G = 2, 3, 8 in the radial direction. It was found that using more points in the circumferential direction for integration of ordinary or transition elements does not improve solution results. Table 4 contains errors in K_{I} values expressed as percentages.

Most conclusions made for one-dimensional case are valid for two-dimensional modeling of crack-tip fields. For two-dimensional meshes that include quarter-point elements around the crack tip and ordinary or transition elements in the rest

Table 4: Errors (percent) in K_{I} values for the two-dimensional asymptotic problem. The mesh consists of 8×8 elements. Crack tip is surrounded by quarter-point elements of radius h. The rest of the semi-circular area is discretized by ordinary or transition elements. Elements (except for quarter-point) are integrated with N_G gauss integration points in the radial direction. Radial element subdivisions: AP – arithmetic progression, EF – equal function difference per element, ED – equal derivative difference per element.

			Q-point and ord. elements			Q-point and transit. elements		
h	Method	N_G	AP	EF	ED	AP	EF	ED
1/8	Displ	2	-0.263	-0.279	-0.264	-0.292	-0.269	-0.262
1/8	Displ	3	-0.280	-0.282	-0.268	-0.264	-0.262	-0.260
1/8	EDI	2	-0.048	-0.025	-0.012	-0.017	-0.027	-0.022
1/8	EDI	3	-0.045	-0.025	-0.016	-0.080	-0.057	-0.025
1/64	Displ	2	0.600		0.638	-0.670		-0.290
1/64	Displ	3	0.236		0.156	0.228		-0.139
1/64	Displ	8	0.190		0.094	0.382		-0.121
1/64	EDI	2	-0.208		0.895	0.115		-0.081
1/64	EDI	3	-0.199		0.416	-0.271		0.046
1/64	EDI	8	-0.193		0.355	-0.365		0.056
1/512	Displ	2	22.898	18.049	18.059	-13.464	-11.315	-0.397
1/512	Displ	3	16.401	12.684	11.644	-3.071	-1.770	0.328
1/512	Displ	8	11.917	9.440	7.849	0.722	1.547	0.534
1/512	EDI	2	-1.116	-0.916	18.361	0.574	0.542	-0.523
1/512	EDI	3	-1.164	-0.975	11.954	-0.005	-0.023	0.474
1/512	EDI	8	-1.128	-0.934	8.156	-0.476	-0.486	0.656

of the computational domain, the following factors improve the accuracy of the stress intensity factor evaluation:

Radial distribution of element sizes providing equal stress difference per element (ED);

Use of transition elements;

Increase of integration order in the radial direction for evaluation of element stiffness matrices.

Accuracy degradation can be attributed to:

Table 5: Errors (percent) in K_{I} values for the two-dimensional asymptotic problem. The mesh consists of $8 \times n_\theta$ elements. The radius of the quarter-point elements is $1/8$. The rest of the semi-circular area is discretized by ordinary or elements. Radial element subdivisions: AP – arithmetic progression, EF – equal function difference per element, ED – equal derivative difference per element.

	Displacement method			EDI method		
$n_r \times n_\theta$	AP	EF	ED	AP	EF	ED
8×4	-1.370	-1.381	-1.389	-0.048	-0.039	-0.064
8×8	-0.263	-0.279	-0.264	-0.048	-0.025	-0.012
8×12	-0.094	-0.114	-0.106	-0.036	-0.013	-0.001
8×16	-0.038	-0.060	-0.055	-0.032	-0.009	0.003
8×24	0.002	-0.022	-0.020	-0.029	-0.006	0.005
8×32	0.015	-0.010	-0.008	-0.028	-0.005	0.006

Decrease of the relative quarter-point element size;

Use of elements with curved sides in the circumferential direction (see Table 3).

The integration order for the quarter-point elements and the number of integration points in the circumferential direction for ordinary or transition elements do not noticeably affect value of the stress intensity factor.

It is most difficult to get acceptable results for small radial sizes of the quarter-point element, for example, $1/n^3$, especially when element sizes do not follow a ED radial distribution. In this case, modeling should be done using quarter-point and transition elements with radial integration rule $N_G = 8$.

Small sizes of quarter-point and neighboring elements can be useful in modeling elastic-plastic crack-tip fields for calculation of second fracture parameter [Nikishkov, Brueckner-Foit, and Munz (1995)] in addition to the J-integral.

3.3.4 Element sizes in the circumferential direction

Selection of radial distribution of element sizes that corresponds to equal increment of stress per element helps to reduce error in K_{I} values. Several attempts were made to improve solution accuracy by changing element sizes in the circumferential direction. For example, it is possible to derive element size distributions which are based on equal increments of displacement $u_\theta(\theta)$ or stress $\sigma_\theta(\theta)$. However, no such attempts improved results. Different components of displacements and stresses follow different angular functions. Because of this, it is probably impossi-

ble to obtain optimal element subdivision in the circumferential direction without increasing the number of subdivisions.

However, it is possible to simply use more elements in the circumferential direction without changing the number of elements in the radial direction. Table 5 juxtaposes errors in the stress intensity factor for meshes with eight elements in the radial direction and variable number of elements n_θ in the circumferential direction. Results show that increasing the number of elements in the circumferential direction by a factor of 1.5–2 considerably improves solution accuracy for all radial distributions of element sizes.

4 Conclusion

The quarter-point element was studied to determine influence of several factors on the accuracy in modeling crack-tip fields. One- and two-dimensional quarter-point elements were applied to problems with inverse square-root singularity that have known solutions.

It is demonstrated that the stiffness matrix of the two-dimensional quarter-point elements contains theoretically unbounded entries except for rows and columns related to quarter-point nodes. Finite values of stiffness coefficients are obtained due to their numerical integration. While coefficient values depend on the integration rule used, solution results are independent of the number of integration points.

To obtain higher accuracy for the stress intensity factor, it is recommended to create meshes with radial distribution of element sizes that provide constant increment of stresses per element and to use transitional elements in addition to quarter-point elements. Use of higher order rules for integration of element stiffness matrices in the radial direction and increasing the number of elements in the circumferential direction also help to improve solution accuracy. Higher order integration in the radial direction is definitely important for meshes with small radial size of quarter-point elements.

The conclusions made on the basis of two-dimensional solutions of the inverse square root problem should be valid for three-dimensional fracture mechanics problems, since asymptotic behavior of displacements and stresses in planes normal to the crack front is similar to that for the two-dimensional case.

Acknowledgement: The author is thankful to Prof. Michael Cohen, University of Aizu, and to Dr. Yuri Nikishkov, University of Texas at Arlington, for their suggestions that improved the paper.

References

Barsoum, R. S. (1976): On the use of isoparametric finite elements in linear fracture mechanics. *International Journal for Numerical Methods in Engineering*, vol. 10, pp. 25–37.

Barsoum, R. S. (1977): Triangular quarter-point elements as elastic and perfectly-plastic crack tip elements. *International Journal for Numerical Methods in Engineering*, vol. 11, pp. 85–98.

Dong, L.; Atluri, S. N. (2013): Fracture & Fatigue Analyses: SGBEM-FEM or XFEM? Part 1: 2D Structures. *CMES: Computer Modeling in Engineering & Sciences*, vol. 90, pp. 91–146.

Dong, L.; Atluri, S. N. (2013): Fracture & Fatigue Analyses: SGBEM-FEM or XFEM? Part 2: 3D solids. *CMES: Computer Modeling in Engineering & Sciences*, vol. 90, pp. 379–413.

Fawkes, A. J.; Owen, D. R. J.; Luxmoore, A. R. (1979): An assessment of crack tip singularity models for use with isoparametric elements. *Engineering Fracture Mechanics*, vol. 11, pp. 143–159.

Harrop, R. P. (1982): The optimum size of quarter-point crack tip element. *International Journal for Numerical Methods in Engineering*, vol. 17, pp. 1101–1103.

Henshell, R. D.; Shaw, K. G. (1975): Crack tip finite elements are unnecessary. *International Journal for Numerical Methods in Engineering*, vol. 9, pp. 495–507.

Hibbitt, H. D. (1977): Some properties of isoparametric elements. *International Journal for Numerical Methods in Engineering*, vol. 11, pp. 180–184.

Lim, I. L.; Johnston, I. W.; Choi, S. K. (1991): The use of transition elements. *Engineering Fracture Mechanics*, vol. 40, pp. 975–983.

Lynn, P. P.; Ingraffea, A. R. (1978): Transition elements to be used with quarter-point crack-tip elements. *International Journal for Numerical Methods in Engineering*, vol. 12, pp. 1031–1036.

Mathematica (2010): *Version 8.0.* Wolfram Research, Inc.

Murti, V.; Valliappan, S. (1986): A universal optimum quarter point element. *Engineering Fracture Mechanics*, vol. 25, pp. 237–258.

Nikishkov, G. P.; Atluri, S. N. (1987): Calculation of fracture mechanics parameters for an arbitrary three-dimensional cracks by the equivalent domain integral method. *International Journal for Numerical Methods in Engineering*, vol. 24, pp. 1801–1821.

Nikishkov, G. P.; Brueckner-Foit, A.; Munz, D. (1995): Calculation of the second fracture parameter for finite cracked bodies using a three-term elastic-plastic asymptotic expansion. *Engineering Fracture Mechanics*, vol. 52, pp. 685–701.

Nikishkov, G. P.; Park, J. H.; Atluri, S. N. (2001): SGBEM-FEM alternating method for analyzing 3D non-planar cracks and their growth in structural components. *CMES: Computer Modeling in Engineering & Sciences*, vol. 2, pp. 401–422.

Saouma, V. E.; Schwemmer, D. (1984): Numerical evaluation of the quarter-point crack tip element. *International Journal for Numerical Methods in Engineering*, vol. 20, pp. 1629–1641.

Wang, H. T.; Yao, Z. H. (2011): A fast multipole dual boundary element method for the three-dimensional crack problems. *CMES: Computer Modeling in Engineering & Sciences*, vol. 72, pp. 115–147.

Yavari, A.; Moyer, E. T. J.; Sarkani, S. (1999): A reappraisal of transition elements in linear elastic fracture mechanics. *International Journal of Fracture*, vol. 100, pp. 227–248.

Ying, L.-A. (1982): A note on the singularity and the strain energy of singular elements. *International Journal for Numerical Methods in Engineering*, vol. 18, pp. 31–39.

Zienkiewicz, O. C. (2005): *The Finite Element Method: Its Basis and Fundamentals*. Elsevier.